Monitoring global changes in chromatin compaction states upon localized DNA damage with tools of fluorescence anisotropy

P. S. Kesavan, Darshika Bohra, Sitara Roy†, and Aprotim Mazumder*
TIFR Centre for Interdisciplinary Sciences, Tata Institute of Fundamental Research Hyderabad, Hyderabad 500046, Telangana, India

ABSTRACT **In the eukaryotic nucleus, DNA, packaged in the form of chromatin, is subject to continuous damage. Chromatin has to be remodeled in order to repair such damage efficiently. But compact chromatin may also be more refractory to damage. Chromatin responses during DNA double-strand break (DSB) repair have been studied with biochemistry or as indirect readouts for the physical state of the chromatin at the site of damage. Direct measures of global chromatin compaction upon damage are lacking. We used fluorescence anisotropy imaging of histone H2B-EGFP to interrogate global chromatin compaction changes in response to localized DSBs directly. Anisotropy maps were preserved in fixation and reported on underlying chromatin compaction states. Laser-induced clustered DSBs led to global compaction of even the undamaged chromatin. Live-cell dynamics could be coupled with fixed-cell assays. Repair factors, PARP1 and PCNA, were immediately recruited to the site of damage, though the local enrichment of PCNA persisted longer than that of PARP1. Subsequently, nodes of PCNA that incorporated deoxynucleotide analogs were observed in regions of low-anisotropy open chromatin, even away from the site of damage. Such fluorescence anisotropy–based readout of chromatin compaction may be used in the investigation of different forms of DNA damage.**

Monitoring Editor
Tom Misteli
National Institutes of Health, NCI

Received: Aug 1, 2019
Revised: Mar 3, 2020
Accepted: Apr 16, 2020

INTRODUCTION

DNA in the eukaryotic cell nucleus is packaged into chromatin with histones and other protein components. This genetic material is susceptible to damage from different sources. It is estimated that in a day, a single mammalian cell can face as many as 100,000 lesions to its DNA (Ciccia and Elledge, 2010). If left unrepaired, such damage can result in cell cycle arrest, cell death, or senescence, or, at the level of the organism, cause mutations that result in diseases such as cancers or neurodegenerative diseases (Friedberg *et al.*, 2006; Madabhushi *et al.*, 2014). To deal with this constant assault on genetic material, cells have evolved a cohort of mechanisms that sense and repair DNA damage (Hoeijmakers, 2009).

Every DNA damage response (DDR) in eukaryotic cells takes place in the context of chromatin. Biochemical studies in in vitro systems with synthetically damaged DNA have helped uncover the critical role that chromatinization plays in DDR. In experiments with purified systems of repair, when a nucleosome was added to the naked DNA, measurements of repair kinetics by nucleotide excision repair (NER) and base excision repair (BER) indicated that the repair was much slower than that of naked DNA without a nucleosome (Hara *et al.*, 2000; Odell *et al.*, 2011). This led to the conclusion that the proteins that help package DNA inside the nucleus can have a hindering effect on damage repair. In cells, regions undergoing repair have been found to be more sensitive to micrococcal nuclease digestion than bulk DNA (Smerdon *et al.*, 1978). This indicates that DNA can be more exposed during damage repair. Proteins that modify nucleosomes, such as SWI/SNF, and histone acetyltransferases (HATs), such as CHD4, have been found to be recruited to the site of damage, which indicates that the chromatin at the site of

This article was published online ahead of print in MBoC in Press (http://www.molbiolcell.org/cgi/doi/10.1091/mbc.E19-08-0417) on April 22, 2020.
Conflicts of interest: The authors declare no conflicts of interest.
†Present address: Section of Cell and Developmental Biology, University of California, San Diego, La Jolla, CA 92093-0335.
*Address correspondence to: Aprotim Mazumder (aprotim@tifrh.res.in).
Abbreviations used: DDR, DNA damage responses; DSB, double-strand break; EdU, ethynyl deoxyuridine; FAI, fluorescence anisotropy imaging.

damage may be relaxed as a response to damage (Park *et al.*, 2006; Polo *et al.* 2010). Further proteins that maintain chromatin integrity, such as KAP-1, have been found to be substrates for the DDR master kinase, ATM (Ziv *et al.*, 2006).

A previous study has found that markers of repair persist in heterochromatin regions for longer time than in euchromatic regions (Goodarzi *et al.*, 2008), indicating that the dynamics of repair is sensitive to the compaction state and activity of chromatin. With core histone H2B tagged with GFP and microirradiation of Hoechst-sensitized cells, it has been shown that chromatin is decompacted at the site of damage in response to clustered double-strand breaks (DSBs), followed by a phase of increased compaction (Kruhlak *et al.*, 2006; Strickfaden *et al.*, 2016). Compaction of chromatin is critical to DDR, and compaction in the absence of damage is sufficient to stimulate a damage response, independent of damage (Burgess *et al.*, 2014). However, in experiments using microscopy, the spreading or shrinking of a chromatin region marked with a specific fluorescent histone has been used as a proxy for chromatin compaction, and as such does not report directly on physical state of the chromatin. In other studies, fluorescence anisotropy imaging (FAI) has been used to map the compaction of chromatin in living cells directly (Banerjee *et al.*, 2006). Core histone H2B tagged with EGFP is excited with polarized light, which preferentially excites EGFP molecules whose excitation dipoles are oriented along the polarization axis of the excitation light. The extent of depolarization of the emission light gives a measure of the rotational diffusion of EGFP fusion proteins. The higher the rotational diffusion, the greater is the extent of depolarization of the emission signal, over and above what would be expected because of random orientations of the fluorophores. Fluorescence anisotropy is a measure of the extent of depolarization (Lakowicz, 2006; Ghosh *et al.*, 2012). Since H2B-EGFP in the regions of euchromatin should have greater rotational mobility than regions of heterochromatin, anisotropy maps generated by FAI show evidence of differential compaction of chromatin and as such could be used as a direct physical measure of local chromatin packaging (Bhattacharya *et al.*, 2009; Makhija *et al.*, 2014). In this study, we sought to use FAI in the context of DDR to monitor chromatin compaction states directly. Chromatin decompaction is essential for repair, and yet local chromatin compaction may be used by cells to prevent further damage (Burgess *et al.*, 2014). Using FAI, we studied the physical changes to the chromatin structure in response to laser microirradiation–induced clustered DSB, in regions of chromatin beyond just the site of damage. We show that anisotropy maps are preserved in fixation and regions of high and low anisotropy indeed correspond to physiologically relevant markers for heterochromatin and euchromatin, respectively. This also allows us to first follow compaction changes in response to localized DSBs in living cells, and then fix the cells and perform immunofluorescence for markers of DNA damage. Finally, we follow the differential dynamics of two endogenous damage-responsive proteins (PCNA and PARP1) with respect to chromatin compaction maps and show that their time scales of recruitment and subsequent dispersion are very different. In addition to being recruited at the site of damage, PCNA also forms nodes further away in regions of low anisotropy. These PCNA nodes in open chromatin incorporate deoxynucleotide analogs, indicating that individual DSBs from the laser-induced cluster may be extruded out from the site of damage for the purposes of repair. Together, these studies open up a new avenue of following DDR in live cells in the chromatin, while also taking advantage of different immunofluorescent markers for DNA damage and chromatin.

RESULTS

Fluorescence anisotropy maps are preserved in fixation and reflect chromatin compaction

The strength of FAI is that it allows the monitoring of chromatin compaction in living cells, but if it can be combined with fixed cell immunofluorescence, it can open up new possibilities of studying DDR on a cell- by-cell basis because of the different antibodies available against damage and chromatin markers. A previous study has shown that nucleosome level mobility is not abrogated by fixation (Hihara *et al.*, 2012). Encouraged by this observation, we wondered whether FA maps may be preserved in fixation. This was indeed the case, and fixing HeLa cells stably expressing H2B-EGFP with 4% paraformaldehyde (PFA) for 15 min did not significantly alter the anisotropy maps (Supplemental Figure 1). While the anisotropy values are dimensionless fractional numbers, and the variation within the nucleus is between 0.10 and 0.19 in the nucleus shown, it should be borne in mind that this range can correspond to a change of between 18 and 215 centipoise in terms of local viscosity for a molecule such as fluorescein (Supplemental Figure 2). Given the good correspondence observed between the live-cell and fixed-cell anisotropy maps, this could potentially enable the combination of anisotropy imaging with immunostaining for different chromatin and DDR marker proteins. Thus, next, we checked the biological relevance of the anisotropy maps generated using markers for euchromatin and heterochromatin. HeLa cells expressing H2B-EGFP were fixed and stained for different heterochromatin and euchromatin markers. Correspondence of these biologically relevant chromatin compaction states with respective anisotropy maps for H2B-EGFP in the same cells was investigated. Trimethylated lysine at the ninth position in core histone protein H3 (H3K9Me3) is a histone modification that is generally associated with densely packed heterochromatin regions (Nakayama *et al.*, 2001). Heterochromatin Protein 1α (HP1α) is associated with heterochromatin domains and is another marker for densely packed chromatin (Lachner *et al.*, 2001). Indeed, corroborating our expectations, line profiles across regions of high levels of H3K9me3 and HP1α showed them to be regions of high anisotropy (Figure 1). Conversely, when we stained cells for decompacted regions of active transcription, using an antibody against the activated form of RNA polymerase, in which S5 is phosphorylated in the C-terminal (Dahmus, 1996) of the largest subunit, we found the regions of stronger phospho-RNAPII staining to be anticorrelated to local anisotropy (Figure 1). We also used mouse NIH 3T3 fibroblast cells that show clear nodes of pericentric heterochromatin. NIH 3T3 cells transiently transfected with H2B-EGFP show high-contrast anisotropy maps, with pericentric heterochromatin in chromocenters corresponding to high-anisotropy regions (Supplemental Figure 3). Together, these results suggest that regions of high and low anisotropy indeed correspond to densely packed heterochromatin and loosely packed euchromatin, respectively.

Overall chromatin compaction changes upon laser microirradiation–induced DSBs

The main strength of FAI is that it can report on chromatin compaction states in living cells. And because anisotropy maps are preserved in fixation, as demonstrated in the previous section, live-cell dynamics upon DNA damage can be followed by immunofluorescent detection of damage markers in the very same cells. We used FAI to study the changes to chromatin structure that has undergone microirradiation induced DSBs as employed by previous studies (Kruhlak *et al.*, 2006; Burgess *et al.*, 2014; Strickfaden *et al.*, 2016). We modified our FAI microscope to introduce a 405-nm laser into

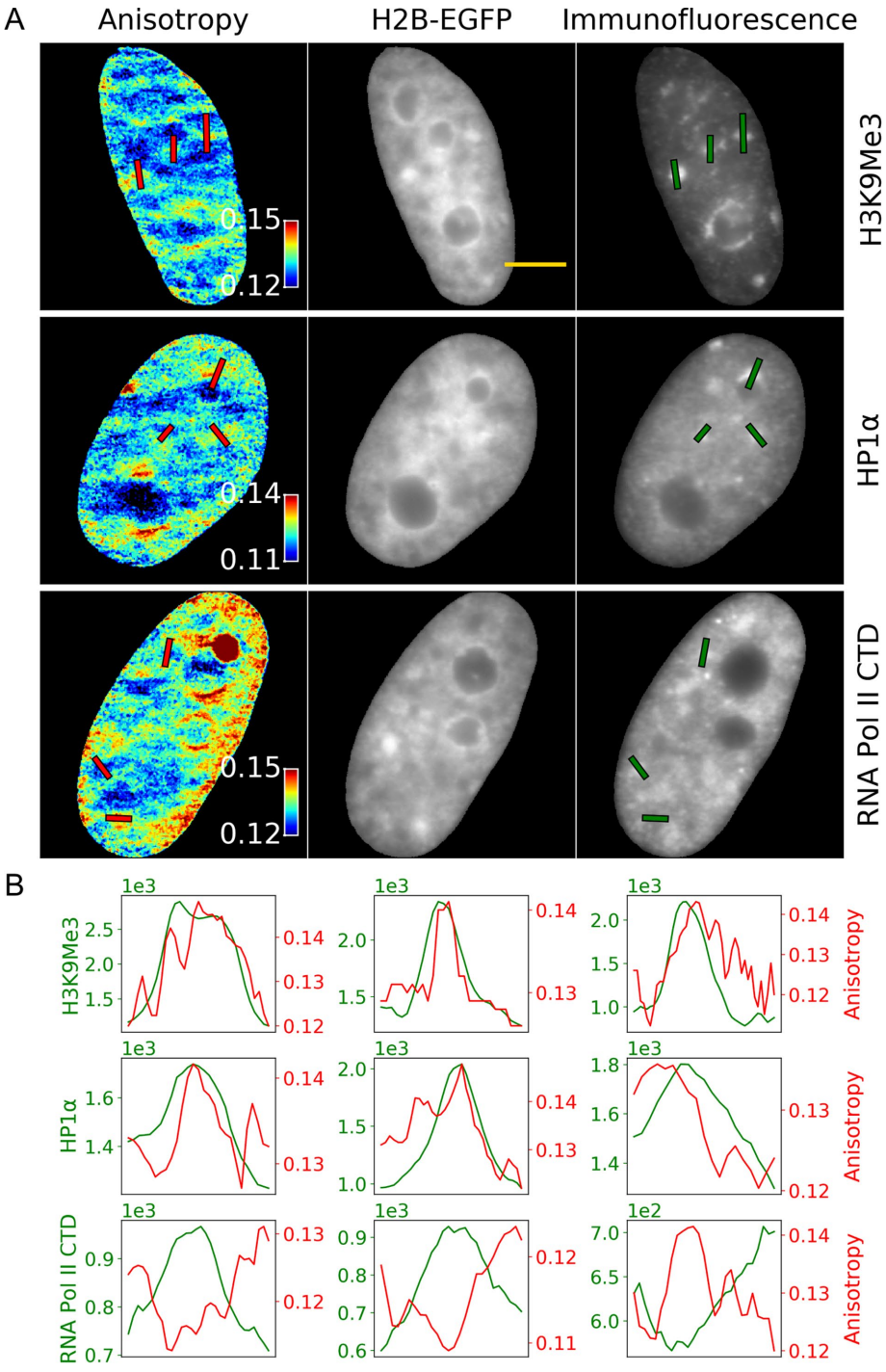

FIGURE 1: H2B-EGFP anisotropy maps corresponds to biologically relevant chromatin compaction states. (A) Anisotropy combined with immunofluorescence of chromatin structure markers. Immunofluorescence against markers of chromatin is imaged along with H2B-EGFP anisotropy images. HP1α and H3K9Me3 are markers of densely packed heterochromatin, and phosphorylated RNA-Pol-II-CTD is a marker of active regions of transcription, the chromatin around which is more open. Scale bar corresponds to 5 μm. (B) Lines (green in the immunofluorescence image, red in the anisotropy image) are drawn in regions of high or low immunofluorescence staining in A, and the corresponding anisotropy and intensity values are plotted, clearly showing that heterochromatin corresponds to regions of high anisotropy, while euchromatin corresponds to regions of low anisotropy. The *x*-axes are distances along the lines.

the light path and used Hoechst-sensitized cells to cause local double-strand breaks of the DNA. Minutes after irradiation, strong staining for γH2AX and the phosphorylated form of Chk1 (p-Chk1, a target of the master DDR kinase ATR) was observed at the site of damage (Supplemental Figure 4), which indicated that the damage response was in action. Using this microirradiation protocol, we collected anisotropy data for the damaged cells over a period of 2 h, imaged once every 5 min. Anisotropy at the site of the damage could not be ascertained due to localized photobleaching of H2B-EGFP upon irradiation, but the response of the rest of the chromatin, which did not see direct irradiation, could be followed. In comparison to the control undamaged cells ($N = 13$), the overall Δanisotropy value (Δanisotropy = $r_t - r_0$, where r_t is the mean anisotropy at any given time point, and r_0 is the mean anisotropy for the 0th time point) of the irradiated cells increased with time (Figure 2B), though the response was heterogeneous among cells (Supplemental Figure 5). And though the mean rise is small, one should keep in mind that anisotropy values are themselves fractional; also, mean anisotropy averages over regions where compaction increases and surrounding regions where it decreases correspondingly, keeping the changes in mean anisotropy small. This heterogeneity is captured in the anisotropy maps, and indeed a fraction of cells show formation of nodes of high local compaction even in regions that have not directly been damaged (Figure 2A). To quantify this better and visualize the nodes, we thresholded the anisotropy map with a threshold value of "mean + 2 sigma," where mean is the mean anisotropy value of the nucleus before damage and sigma is the SD. Values below the threshold are turned to gray, so that it becomes easier to visualize the high–anisotropy value pixels formed upon irradiation (Supplemental Figure 5C). The formation of high-anisotropy nodes is reflected in the overall increase in high-anisotropy pixels for irradiated cells as compared with control cells. However, it should be noted that the control cells also show a fair degree of heterogeneity among themselves, and this could be because of toxic effects of the imaging excitation light (Ge *et al.*, 2013), natural cell cycle–driven processes that causes chromatin compaction changes, or systematic changes to anisotropy with photobleaching. Nonetheless, the propensity for increased compaction in irradiated cells is clear and significantly different from the dynamics of control cells. When the individual Δanisotropy time trace for each irradiated cell is examined closely (Supplemental Figure 5), 21 out of 27 cells show positive increase in delta anisotropy and only 6 out of 27 cells show an overall negative trend over the 2 h after damage, whereas in control cells, 7 out of 13 cells show a positive trend and 6 out of

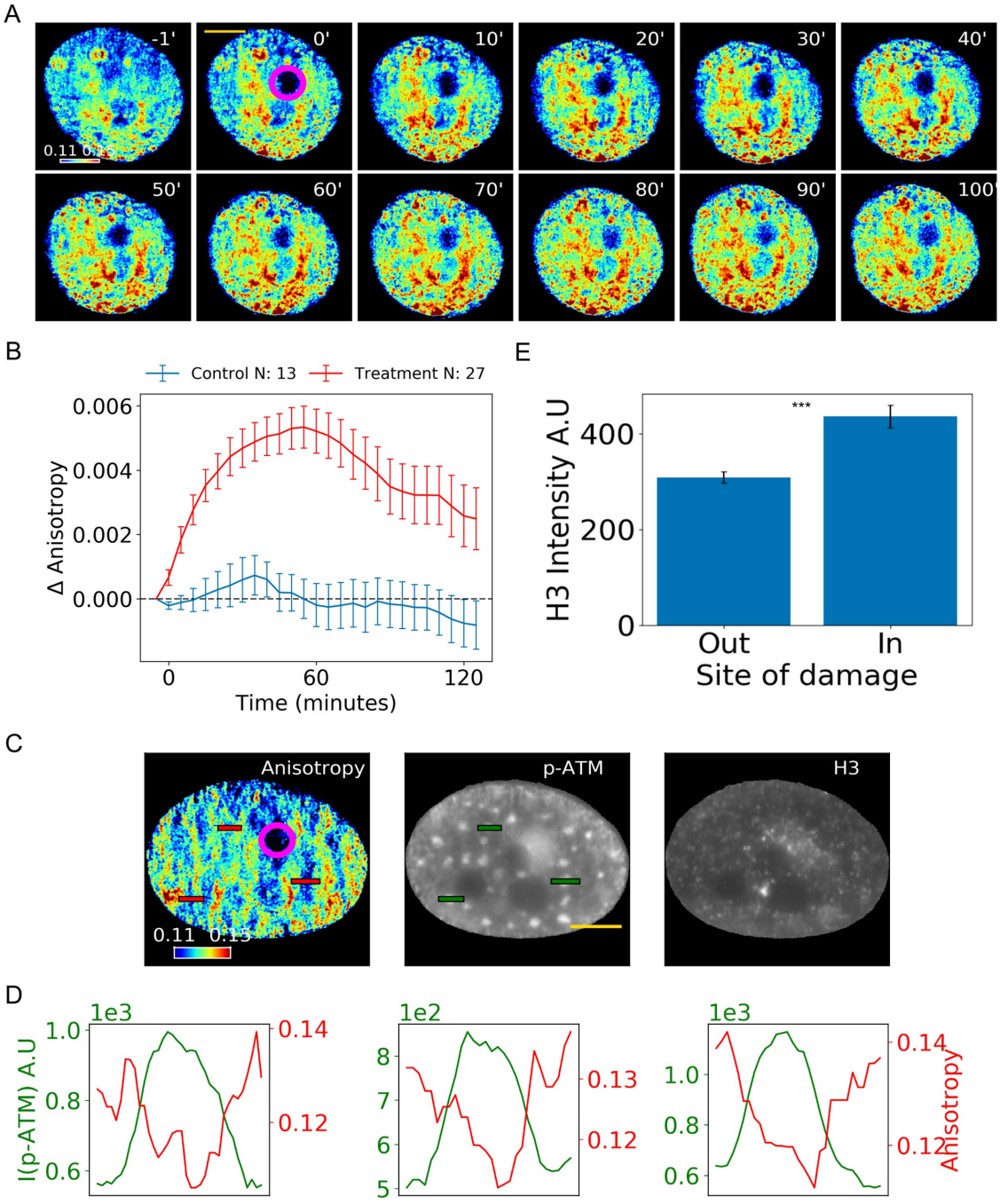

FIGURE 2: Dense nodes of chromatin are formed in microirradiated cells. (A) H2B-EGFP anisotropy time series for a representative irradiated cell before and after irradiation, imaged every 5 min for over 2 h. Scale bar corresponds to 5 μm. The color map is scaled from 0.11 to 0.15. (B) Δanisotropy for any time trace is calculated by subtracting the mean H2B-EGFP anisotropy of the nucleus for a given time point from the mean H2B-EGFP anisotropy of the first time point. A positive change in Δanisotropy corresponds to chromatin compaction, and a negative change corresponds to decompaction. Mean changes are calculated for control ($N = 13$) and irradiated cells ($N = 27$). Error bars represent standard errors of mean. Individual time traces are also shown in Supplemental Figure 5. (C) H2B-EGFP anisotropy image for an irradiated cell, 2 h after irradiation, immunostained for phosphorylated-ATM and core histone protein, H3. Color map in anisotropy map is scaled from 0.11 to 0.15. Scale bar corresponds to 5 μm. (D) Line profiles show that anisotropy values are anticorrelated with phosphorylated ATM intensity values. The *x*-axes are distance along the lines shown (green in the immunofluorescence image, red in the anisotropy image). (E) Immunofluorescence against H3 shows enrichment at the site of damage. *** implies $p < 0.001$ by Student's *t*-test ($p = 2.45e\text{-}05$ for $N = 18$). Magenta circles indicate the sites of microirradiation.

13 cells show a negative trend. This indicates that there is inherent variability in the cellular response to damage, but overall there is condensation of chromatin in response to damage.

Following the measurement of chromatin compaction dynamics, we could perform immunofluorescence for DDR markers in the very same cells. We observed that the phosphorylated form of the

master kinase, ATM, forms nodes throughout the nucleus in a fraction of damaged cells (Figure 2C). These nodes are exclusively formed in regions of low anisotropy, perhaps indicating that these may be sites permissive for repair. The core histone protein H3 on the other hand shows a somewhat stronger staining at the site of damage, where anisotropy cannot be measured. This may indicate increased chromatin compaction at the site of damage, as has been reported before (Polo *et al.*, 2006; Ayrapetov *et al.*, 2014), and is a reflection of the compaction changes at the site of damage. The possibility of following chromatin compaction dynamics by immunofluorescent detection of damage response markers in the same cells is clearly demonstrated by these experiments.

PCNA and PARP1 dynamics in irradiated cells

Next we wanted to combine the time course of anisotropy imaging with live-cell detection of other markers of the damage response. For this, we chose chromobody-mediated detection of early and late markers of DDR—PARP1 and PCNA. PARP1 is known to be transiently enhanced at sites of damage in response to irradiation-induced DSBs (Chou *et al.*, 2010; Qi *et al.*, 2019), while PCNA, being the DNA clamp, would be required for the processivity of the DNA polymerase in the final steps of repair (Moldovan *et al.*, 2007). We independently transfected PARP1 and PCNA chromobodies tagged with TagRFP in HeLa cells stably expressing H2B-EGFP. Chromobodies (ChromoTek) are small intracellular antibodies tagged with fluorescent protein. Their major advantage is that they detect the endogenous proteins they are designed against without artifacts of overexpression of those proteins in transient transfections (Burgess *et al.*, 2012; Panza *et al.*, 2015). As expected, PARP1 was recruited to the site of damage almost immediately upon irradiation (Figure 3A). However, the PARP1 signal diffused away from the site by 15 min after damage, as expected (Haince *et al.*, 2008; Mortusewicz *et al.*, 2007). To our surprise, however, PCNA, which should be involved in the repair only at later stages, was also recruited immediately to the site of damage (Figure 3B). This was the case in G1 and G2 cells where the PCNA chromobody was homogenous in the nucleus, and even in S phase cells where the PCNA chromobody was punctated, as PCNA follows the replication fork (Supplemental Movies 1 and 2). The PCNA chromobody is primarily used for cell-cycle stage detection (Burgess *et al.*, 2012). This implies that in response to clustered DSBs, even PCNA from replication forks is recruited to the site of damage. PCNA persisted at the site of damage for the duration of the time course, longer than PARP1 (Figure 3C). This local enrichment was quantified by plotting the mean intensity of the chromobody at the site of damage normalized to the mean intensity outside. (We found this to be a more robust metric for the enrichment, compared with just the normalized intensity at the site of damage, which decays due to photobleaching during the time course, in addition to actual dynamics. This metric is more robust because photobleaching operates both within and outside the site of damage.) But while PCNA persists longer, within 20 min, there are nodes of PCNA formed, away from the site of damage, which correspond to regions of lower anisotropy (Figure 3; Supplemental Figure 6). We asked whether these sites of PCNA enrichment and low anisotropy represent simply sites of repair factor storage or of active repair. We reasoned that if they are indeed sites of repair, even in the G1 or G2 phase, we may be able to see incorporation of a deoxynucleotide analog such as ethynyl deoxyuridine (EdU). HeLa cells transfected with the PCNA chromobody were subjected to laser-induced DSBs. G1 or G2 cells that have a homogenous distribution of the PCNA chromobody in the nucleus were chosen. We observed that at these sites of transient PCNA nodes, EdU is incorporated, which is an indication of new DNA being synthesized at these sites (Figure 3E; Supplemental Figure 7). We ruled out bleedthrough of PCNA signal in the EdU channel by imaging plates for cells with and without EdU treatment (Supplemental Figure 7). Thus, though the DSBs are induced locally, these nodes of PCNA incorporating EdU further away may indicate a looping out of individual DSBs from the site of primary damage.

DISCUSSION

Steady-state fluorescence anisotropy imaging has been used previously for measuring chromatin compaction in living cells (Banerjee *et al.*, 2006). We established that anisotropy maps are preserved in fixation, and regions of high and low anisotropy indeed correspond to heterochromatin and euchromatin, respectively. In the context of DDR, our fluorescence anisotropy imaging studies suggest that the undamaged chromatin is globally compacted in response to localized DSB damage. In regions away from the site of damage, we observe chromatin nodes forming, as well as transient accumulation of phospho-ATM and PCNA in specific sites that correspond to more loosely packed regions of chromatin. These low-anisotropy regions with accumulated repair proteins could be regions of repair or of factors poised for repair. In future studies, we aim to investigate the possibility of blocking damage response in cells using small molecule inhibitors for DDR master kinases and what effects it has on the chromatin response upon damage. A limitation of this study is that we follow the response of undamaged chromatin because of local clustered DSBs, but anisotropy information is lost at the site of damage because of photobleaching. This could potentially be circumvented by using a histone H2B tagged with photoactivable GFP (H2B-PA-GFP). Condensation of the damaged chromatin could indeed be observed in such an experiment (Supplemental Figure 8).

We noticed that within 2 min after microirradiation, there is phosphorylation of Ser139 of the histone variant H2AX at the site of microirradiation, indicating DNA damage (Supplemental Figure 4). Although γH2AX is a DNA damage marker, which is generally found as foci in regions of damaged chromatin, there is also a pan-nuclear spreading of γH2AX in undamaged chromatin as early as 5 min after damage. In another study, interference with chromatin compaction at the damage site reduces the efficiency of damage repair. This suggested that condensation of chromatin is a necessary step in the activation of DDR (Burgess *et al.*, 2014). However, ATM activation in mouse fibroblasts showed chromatin opening independent of DNA damage (Ji *et al.*, 2017). During damage, ATM is thought to be activated not by direct binding to DNA strand breaks, but by changes in chromatin structure. Thus, forced compaction of chromatin promotes activation of ATR and ATM even where there are no strand breaks (Burgess *et al.*, 2014), and conversely, activation of these kinases can change chromatin compaction (Becker *et al.*, 2014). Thus, pan-nuclear induction of DDR (for which γH2AX is a proxy) can drive compaction of undamaged chromatin, and the processes could feed back onto each other.

Such pan-nuclear induction of γH2AX has been reported before when clustered DNA damage was induced by ionizing radiation, which is regulated by ATM and DNA-PK (Meyer *et al.*, 2013). Other studies have discussed a ring of γH2AX in the context of apoptosis (Solier and Pommier, 2014). It is possible that some of the cells we have irradiated will undergo apoptosis, and apoptotic response over and above the DNA damage response complicates the observed chromatin phenotypes. But apoptosis is accompanied by visible changes in the cell and nuclear morphology. However, our

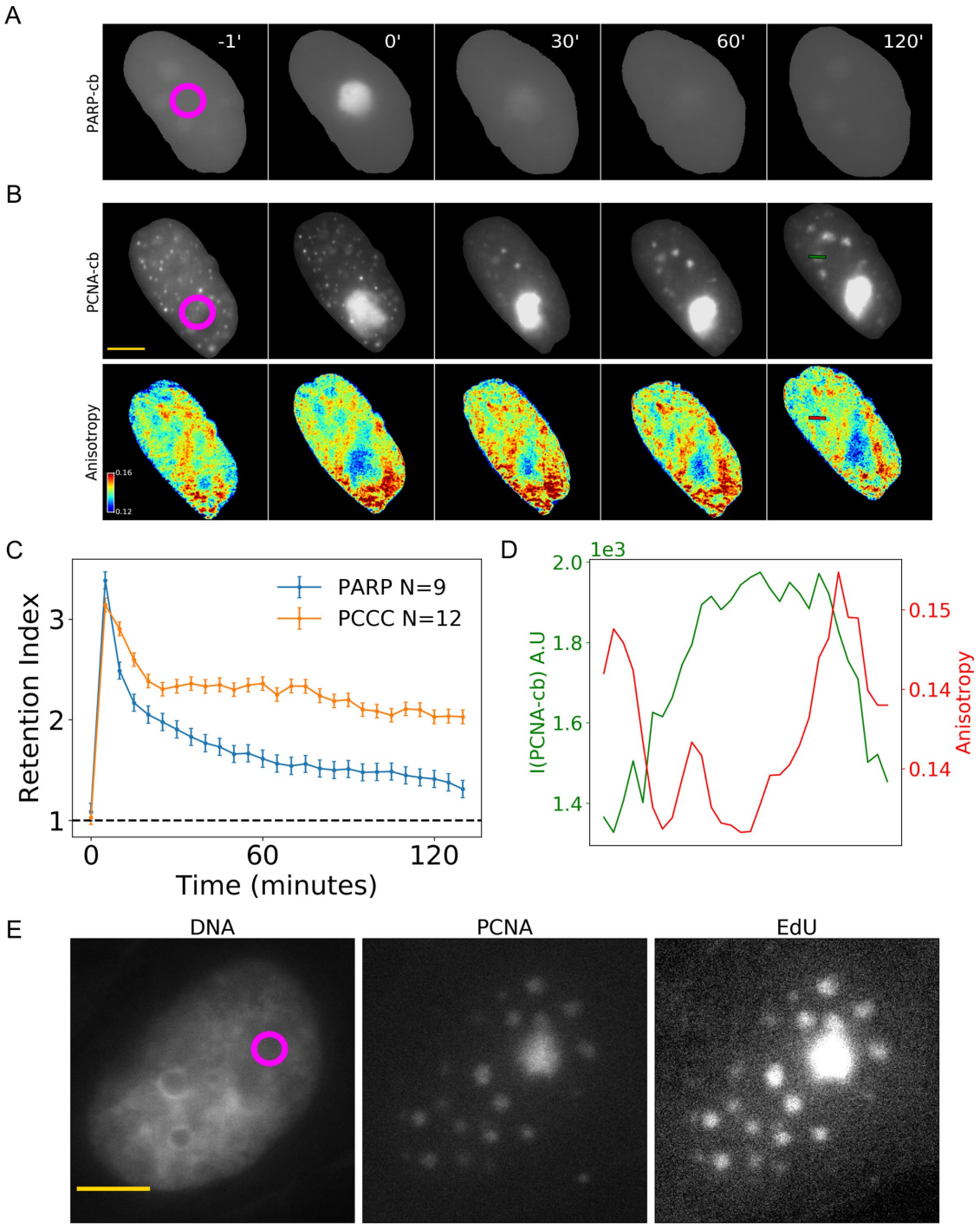

FIGURE 3: Live-cell dynamics of PCNA and PARP in irradiated cells. (A) Representative Hela H2B-EGFP cell expressing PARP-chromobody, imaged at an interval of 5 min postirradiation. PARP1 shows transient enrichment at the site of damage and becomes homogeneous quickly. (B) Representative Hela H2B-EGFP cell expressing PCNA-chromobody, and its corresponding anisotropy maps, imaged at an interval of 5 m postirradiation. The representative time points shown in B are the same as those in A. (C) The retention index for any time point is defined as the ratio of intensity for a chromobody at the site of damage and outside the site of damage. A retention index of 1 indicates a uniform distribution of the chromobody. PCNA shows >twofold retention even at 120 min, while PARP1 tends to come back to baseline faster. *N* indicates the number of cells for time-course experiments. The error bars are standard errors of the mean. (D) Line profile of anisotropy and PCNA at the site of a PCNA node marked by a line at the 120-mie time point in B (green in the PCNA image, red on the anisotropy image). The *x*-axis is distance along the line. Additional line plots may be found in Supplemental Figure 6. Nodes of PCNA form at regions of low anisotropy, that is, open chromatin. (E) Sites of PCNA accumulation show EdU incorporation even outside the site of damage. Images of DNA stained with Hoechst, PCNA chromobody labeled with TagRFP, and EdU detected with Cy5 Azide are shown. The magenta circles indicate sites of microirradiation-induced damage in A, B, and E. Scale bars correspond to 5 μm.

irradiated cells, under similar irradiation conditions, do not exhibit apoptotic morphology or fragmented chromatin, and many survive 48 h after irradiation. Furthermore, during the 2-h time course over which the cells were imaged, there was no significant induction of apoptotic or general cell death markers (Supplemental Figure 9). This indicates that the compaction we observe may have to do with the early processes of DDR rather than the long-term processes of cell death because of excessive DNA damage.

PCNA, surprisingly, is shown to be recruited immediately to the site of localized DSBs, independent of cell-cycle phase. As interestingly, at longer time-points it forms transient nodes of repair away from the site of damage in regions of more open chromatin (low anisotropy). These nodes actively incorporate EdU, indicating active repair and possibly a looping of DSBs from the primary laser-induced cluster to open regions of chromatin for the purposes of repair.

Our study establishes the possibility of using FAI to measure chromatin compaction changes in the context of DNA damage in living cells, followed by immunofluorescence for DDR and chromatin markers. While the response to DSBs is investigated here, following previous studies (Kruhlak *et al.*, 2006; Burgess *et al.*, 2014), in principle, the method is amenable to other forms of DNA damage as well, which we aim to investigate in the future.

MATERIALS AND METHODS

Cell culture and plasmids

HeLa and NIH 3T3 cells were procured from the National Centre for Cell Science (NCCS), the national cell line repository of India. FAI experiments have been performed on HeLa cells before (Banerjee *et al.*, 2006). Cells were grown in DMEM/F12 supplemented with 10% FBS and 1% PenStrep-glutamate in an Eppendorf Galaxy 170S CO_2 incubator maintained at 37°C and 5% CO_2. Cell culture reagents were procured from Life Technologies, ThermoFisher Scientific. For imaging, cells were grown in 35-mm glass-bottomed dishes (Genetix, 200350) and imaged in FluoroBrite medium (Life Technologies, ThermoFisher Scientific, A1896701). The FluoroBrite medium is specially formulated for live-cell imaging with low backgrounds. The H2B-EGFP plasmid was a gift from Geoff Wahl (Addgene plasmid #11680; http://n2t.net/addgene:11680; RRID:Addgene_11680; Kanda *et al.*, 1998). HeLa cells stably expressing H2B-EGFP were selected with geneticin. Plasmids for PCNA chromobody, pCCC-TagRFP (ccr), and PARP1-Chromobody-TagRFP (xcr) were purchased from ChromoTek. Cells were transfected with X-tremeGENE HP DNA transfection reagent (Sigma Aldrich, Roche, XTGHP-RO). Chromobody experiments were performed as transient transfections in the HeLa cell line stably expressing H2B-EGFP unless otherwise mentioned. Cells were tested to be mycoplasma-free.

Microirradiation

Cells growing in 35-mm glass-bottomed dishes were stained with 1 µg/ml Hoechst for 10 min in FluoroBrite imaging medium (supplemented with 10% FBS and 1% PenStrep-glutamate) and after staining, left to equilibrate in the incubator with FluoroBrite imaging medium for at least 30 min before imaging. The plate was positioned in the microscope so that the 405-nm laser (at 10 mW) was focused on the cell that was to be irradiated. A single location in the nucleus was irradiated for 1.5 s.

Immunofluorescence

Cells were fixed with 4% paraformaldehyde for 15 min, followed by 30 min of permeabilization with 0.1% Triton X-100. A 5% BSA solution in PBS was used for blocking for an hour before the cells were incubated overnight with primary antibodies at 4°C (anti-RNA polymerase II CTD repeat YSPTSPS [phospho S5], abcam ab513 at 1:1000 dilution, anti-phospho-histone H2AX [Ser139; anti-γH2AX], clone JBW301, Merck 05-636 at 1:1000 dilution, anti-Chk1 [phospho S345] antibody, abcam ab47318 at 1:500 dilution, anti-HP1α antibody, clone15.19s2, Merck 05-689 at 1:1000 dilution, anti-trimethyl-histone H3 [Lys9; D4W1U], Cell Signalling Technology 13969 at 1:800, anti-ATM [phospho S1981], abcam ab36810 at 1:500 dilution, Histone H3 [D1H2] XP, Cell Signalling Technology 4499 at 1:500 dilution). Fluorescent-tagged secondary antibodies (Alexa Fluor 546 goat anti-mouse/rabbit [A11030/A11010] and Alexa Fluor 647 goat anti-mouse/rabbit [A21236/A21245]) were incubated at room temperature for 1 h before imaging.

EdU staining

1 µM EdU was added along with the live-cell imaging media and the cells were microirradiated. After the experiment, the cells were fixed and permeabilized as done for immunofluorescence, followed by staining for 30 min with Cy5 Azide dye in a buffer containing HEPES, ammonium guanidine (100 mM), copper sulfate (100 mM), THPTA (50 mM), and sodium ascorbate (1 M) following previous protocols (Presolski *et al.*, 2011; Yang *et al.*, 2013; Ding *et al.*, 2014).

Microscopy

All images were recorded in a modified Olympus IX83 (Tokyo, Japan) with a 100 × 1.4 NA objective and an Andor Zyla 4.2 sCMOS camera with an effective pixel size of 65 nm in the images. CoolLED pE-4000 was used as the light source. Olympus IX83-ZDC2 was used to correct focus drift and an Olympus IX3-SSU ultrasonic stage was used for multipoint imaging. An Olympus double lamp housing U-DULHA was used to introduce a 405-nm diode laser used in microirradiation. An Okolab UNO (Naples, Italy) live-cell chamber supplied with humidified CO_2 and an objective heater was used.

Fluorescence anisotropy imaging and analysis

A linear sheet polarizer was placed after the excitation filter in the filter cube, aligned to polarize light in the vertical direction. An Optosplit II (Cairn Research, Kent, England) with a polarizing beam splitter was attached to the left port of the IX83 frame. The field of view was reduced using apertures and the parallel and perpendicular components of the emission light were projected on two halves of the camera chip, allowing simultaneous recording.

The parallel and perpendicular channels were segmented out and aligned with a fully automated image processing pipeline. Background subtraction of the images was performed. Anisotropy, r, was calculated using the formula

$$r = \frac{(I_{par} - G \times I_{perp})}{(I_{par} + 2 \times G \times I_{perp})}$$

where I_{par} is the intensity of the parallel channel and I_{perp} the intensity of the perpendicular channel, and G is the correction factor for any bias in observation between the parallel and perpendicular channels. G is calculated such that the anisotropy of fluorescein in aqueous buffer is zero.

Δanisotropy is defined as $\Delta r = r_t - r_0$ for a time series, where r_0 is the mean anisotropy value for a cell at the 0th time point and r_t is the mean anisotropy value at any given time point. The retention index is defined as the ratio of the intensity at the site of damage to the intensity outside the site of damage, as defined in the PARP1 and PCNA experiments.

Software

Image were processed with custom functions written in python, borrowing heavily from open source python libraries, such as matplotlib, scikit-image, numpy, and scipy. All the code used in analysis is available in github (https://github.com/pskeshu/fai).

ACKNOWLEDGMENTS

We acknowledge intramural research funds from DAE at TIFR Hyderabad to A.M. and TIFR graduate student fellowships to P.S.K. and D.B. S.R. was supported by a DST Science and Engineering Research Board (SERB) National Post Doctoral Fellowship (N-PDF) scheme (PDF/2016/002781). This research was also partially supported by a SERB Early Career Research Award (ECR/2016/000907) to A.M.

REFERENCES

Ayrapetov MK, Gursoy-Yuzugullu O, Xu C, Xu Y, Price BD (2014). DNA double-strand breaks promote methylation of histone H3 on lysine 9 and transient formation of repressive chromatin. Proc Natl Acad Sci 111, 9169–9174. https://doi.org/10.1073/pnas.1403565111.

Banerjee B, Bhattacharya D, Shivashankar GV (2006). Chromatin structure exhibits spatio-temporal heterogeneity within the cell nucleus. Biophys J 91, 2297–2303.

Becker A, Durante M, Taucher-Scholz G, Jakob B (2014). ATM alters the otherwise robust chromatin mobility at sites of DNA double-strand breaks (DSBs) in human cells. PLoS One 9, e92640. https://doi.org/10.1371/journal.pone.0092640.

Bhattacharya D, Talwar S, Mazumder A, Shivashankar GV (2009). Spatio-temporal plasticity in chromatin organization in mouse cell differentiation and during *Drosophila* embryogenesis. Biophys J 96, 3832–3839.

Burgess A, Lorca T, Castro A (2012). Quantitative live imaging of endogenous DNA replication in mammalian cells. PLoS One 7, e45726.

Burgess RC, Burman B, Kruhlak MJ, Misteli T (2014). Activation of DNA damage response signaling by condensed chromatin. Cell Rep 9, 1703–1717.

Chou DM, Adamson B, Dephoure NE, Tan Xu, Nottke AC, Hurov KE, Gygi SP, Colaiácovo MP, Elledge SJ (2010). A chromatin localization screen reveals poly (ADP ribose)-regulated recruitment of the repressive polycomb and NuRD complexes to sites of DNA damage. Proc Natl Acad Sci USA 107, 18475–18480.

Ciccia A, Elledge SJ (2010). The DNA damage response: making it safe to play with knives. Mol Cell 40, 179–204.

Dahmus ME (1996). Reversible phosphorylation of the C-terminal domain of RNA polymerase II. J Biol Chem 271, 19009–19012. https://doi.org/10.1074/jbc.271.32.19009.

Ding X, Ge D, Yang K-L (2014). Colorimetric protease assay by using gold nanoparticles and oligopeptides. Sens Actuators B Chem 201, 234–239. https://doi.org/10.1016/j.snb.2014.05.014.

Friedberg EC, Walker GC, Siede W, Wood RD, Schultz RA, Ellenberger T (2006). DNA Repair and Mutagenesis. Washington, DC: American Society for Microbiology Press.

Ge J, Wood DK, Weingeist DM, Prasongtanakij S, Navasumrit P, Ruchirawat M, Engelward BP (2013). Standard fluorescent imaging of live cells is highly genotoxic. Cytometry A 83, 552–560.

Ghosh S, Saha S, Goswami D, Bilgrami S, Mayor S (2012). Dynamic imaging of homo-FRET in live cells by fluorescence anisotropy microscopy. Methods in Enzymology, 505, 291–327. https://doi:10.1016/B978-0-12-388448-0.00024-3.

Goodarzi AA, Noon AT, Deckbar D, Ziv Y, Shiloh Y, Löbrich M, Jeggo PA (2008). ATM signaling facilitates repair of DNA double-strand breaks associated with heterochromatin. Mol Cell 31, 167–177. https://doi.org/10.1016/j.molcel.2008.05.017.

Haince J-F, McDonald D, Rodrigue A, Déry U, Masson J-Y, Hendzel MJ, Poirier GG (2008). PARP1-dependent kinetics of recruitment of MRE11 and NBS1 proteins to multiple DNA damage sites. J Biol Chem 283, 1197–1208. https://doi.org/10.1074/jbc.m706734200.

Hara R, Mo J, Sancar A (2000). DNA damage in the nucleosome core is refractory to repair by human excision nuclease. Mol Cell Biol 20, 9173–9181.

Hihara S, Pack C-Gi, Kaizu K, Tani T, Hanafusa T, Nozaki T, Takemoto S, Yoshimi T, Yokota H, Imamoto N, *et al.* (2012). Local nucleosome dynamics facilitate chromatin accessibility in living mammalian cells. Cell Rep 2, 1645–1656.

Hoeijmakers JHJ (2009). DNA damage, aging, and cancer. N Engl J Med 361, 1475–1485. https://doi.org/10.1056/nejmra0804615.

Ji S, Zhu L, Gao Y, Zhang X, Yan Y, Cen J, Li R, Zeng R, Liao L, Hou C, *et al.* (2017). Baf60b-mediated ATM-p53 activation blocks cell identity conversion by sensing chromatin opening. Cell Res 27, 642–656.

Kanda T, Sullivan KF, Wahl GM (1998). Histone–GFP fusion protein enables sensitive analysis of chromosome dynamics in living mammalian cells. Curr Biol 8, 377–385. https://doi.org/10.1016/s0960-9822(98)70156-3.

Kruhlak MJ, Celeste A, Dellaire G, Fernandez-Capetillo O, Müller WG, McNally JG, Bazett-Jones DP, Nussenzweig A (2006). Changes in chromatin structure and mobility in living cells at sites of DNA double-strand breaks. J Cell Biol 172, 823–834. https://doi.org/10.1083/jcb.200510015.

Lachner M, O'Carroll D, Rea S, Mechtler K, Jenuwein T (2001). Methylation of histone H3 lysine 9 creates a binding site for HP1 proteins. Nature 410, 116–120. https://doi.org/10.1038/35065132.

Lakowicz JR, ed. (2006). Principles of Fluorescence Spectroscopy. Boston: Springer US.

Madabhushi R, Pan L, Tsai Li-H (2014). DNA damage and its links to neurodegeneration. Neuron 83, 266–282. https://doi.org/10.1016/j.neuron.2014.06.034.

Makhija E, Iyer K, Talwar S, Shivashankar GV (2014). Probing chromatin structure and dynamics using fluorescence anisotropy imaging. In: Handbook of Imaging in Biological Mechanics, eds. CP Neu, GM Genin, Boca Raton: CRC Press, 391–400.

Meyer B, Voss K-O, Tobias F, Jakob B, Durante M, Taucher-Scholz G (2013). Clustered DNA damage induces pan-nuclear H2AX phosphorylation mediated by ATM and DNA-PK. Nucleic Acids Res 41, 6109–6118.

Moldovan G-L, Pfander B, Jentsch S (2007). PCNA, the maestro of the replication fork. Cell 129, 665–679.

Mortusewicz O, Amé J-C, Schreiber V, Leonhardt H (2007). Feedback-regulated poly(ADP-ribosyl)ation by PARP-1 is required for rapid response to DNA damage in living cells. Nucleic Acids Res 35, 7665–7675. https://doi.org/10.1093/nar/gkm933.

Nakayama J-I, Rice JC, Strahl BD, David Allis C, Grewal SIS (2001). Role of histone H3 lysine 9 methylation in epigenetic control of heterochromatin assembly. Science 292, 110–113. https://doi.org/10.1126/science.1060118.

Odell ID, Barbour J-E, Murphy DL, Della-Maria JA, Sweasy JB, Tomkinson AE, Wallace SS, Pederson DS (2011). Nucleosome disruption by DNA ligase III-XRCC1 promotes efficient base excision repair. Mol Cell Biol 31, 4623–4632. https://doi.org/10.1128/mcb.05715-11.

Panza P, Maier J, Schmees C, Rothbauer U, Söllner C (2015). Live imaging of endogenous protein dynamics in zebrafish using chromobodies. Development 142, 1879–1884.

Park Ji-H, Park E-J, Lee H-S, Kim SoJ, Hur S-K, Imbalzano AN, Kwon J (2006). Mammalian SWI/SNF complexes facilitate DNA double-strand break repair by promoting γ-H2AX induction. EMBO J. https://doi.org/10.1038/sj.emboj.7601291.

Polo SE, Kaidi A, Baskcomb L, Galanty Y, Jackson SP (2010). Regulation of DNA-damage responses and cell-cycle progression by the chromatin remodelling factor CHD4. EMBO J 25, 3986–3997. https://doi.org/10.1038/emboj.2010.188.

Polo SE, Roche D, Almouzni G (2006). New histone incorporation marks sites of UV repair in human cells. Cell 127, 481–493.

Presolski SI, Hong VuP, Finn MG (2011). Copper-catalyzed azide-alkyne click chemistry for bioconjugation. Curr Protoc Chem Biol 3, 153–162. https://doi.org/10.1002/9780470559277.ch110148.

Qi H, Price BD, Day TA (2019). Multiple roles for mono- and poly(ADP-ribose) in regulating stress responses. Trends Genet 35, 159–172.

Smerdon MJ, Tlsty TD, Lieberman MW (1978). Distribution of ultraviolet-induced DNA repair synthesis in nuclease sensitive and resistant regions of human chromatin. Biochemistry 17, 2377–2386. https://doi.org/10.1021/bi00605a020.

Solier S, Pommier Y (2014). The Nuclear γ-H2AX apoptotic ring: implications for cancers and autoimmune diseases. Cell Mol Life Sci 71, 2289–2297.

Strickfaden H, McDonald D, Kruhlak MJ, Haince J-F, Th'ng JPH, Rouleau M, Ishibashi T, Corry GN, Ausio J, Underhill DA, *et al.* (2016). Poly(ADP-ribosyl)ation-dependent transient chromatin decondensation and histone displacement following laser microirradiation. J Biol Chem 291, 1789–1802.

Yang Y, Yang X, Verhelst S (2013). Comparative analysis of click chemistry mediated activity-based protein profiling in cell lysates. Molecules 18, 12,599–12,608. https://doi.org/10.3390/molecules181012599.

Ziv Y, Bielopolski D, Galanty Y, Lukas C, Taya Y, Schultz DC, Lukas J, Bekker-Jensen S, Bartek J, Shiloh Y (2006). Chromatin relaxation in response to DNA double-strand breaks is modulated by a novel ATM- and KAP-1 dependent pathway. Nat Cell Biol 8, 870–876. https://doi.org/10.1038/ncb1446.